Journal of the Nivar Volume 49, Special Issue, Autumn 2025 and Winter 2026, P. 42-54

Homepage: https://nivar.irimo.ir (Research Article)

Investigating the Influence of Salinity and Temperature on the Dispersion of Desalination Brine in a Hypothetical Lake

Hosseini Hamid, M.[1]✉ | Akmarinasab, M.[2] | Layeghi, B.[3]

1. Ph D. Student University of Hormozgan ,Department of Non-Living Atmospheric and Marine Science, Faculty of Marine Science and Technology, University of Hormozgan, Bandar Abbas, Iran.
2. Associate Professor University of Mazandaran, Faculty of Marine and Environmental Sciences, Babolsar, Iran.
3. Director General of the Center for Atmospheric and Oceanic Sciences and Secretary of the Supreme Council of Oceanography, Tehran, Iran.

Corresponding Author E-mail: majidfizik@gmail.com

(Received: 05 Jan 2026, Revised: 15 Jan 2026, Accepted: 227 Jan 2026, Published online: 23 Sep 2026)

Abstract

Seawater desalination has become one of the most effective solutions for freshwater production; however, the return brine discharged into the marine environment represents a significant ecological concern. In this study, the three-dimensional ROMS numerical model was employed to construct an idealized rectangular marine domain in which a surface brine outfall with variable salinity and temperature was released. The seabed slope was assumed constant, with a maximum depth of 150 m, and an eastward surface wind was applied in all scenarios.
In the first case, where the effluent represented a thermally enriched brine discharged at the surface with a temperature of 50 °C, salinity of 40 ppt, and a flow rate of 2 m³/s, the brine plume remained predominantly near the surface, advected forward under the influence of wind. No evidence of brine reaching the seabed was observed. Increasing the brine salinity to 45 ppt did not significantly alter its vertical movement; however, surface spreading expanded toward the coast, resulting in plume accumulation in two shoreline regions.
In the scenario with an effluent temperature of 45 °C, salinity of 55 ppt, and a discharge rate of 1 m³/s, the brine mass became sufficiently dense to sink and travel along the seabed, posing a potential threat to benthic ecosystems. Overall, the findings indicate that low-density effluents are primarily governed by wind-driven circulation, whereas increased brine density enhances downward movement toward the seabed.
In an additional application of ROMS, a high-density reverse osmosis brine discharge was simulated for a coastal point along the western Sea of Oman, released at the surface with a flow rate of 10 m³/s. Model results showed a two-branch transport pathway: one part of the plume progressed toward the Strait of Hormuz, while the other was advected offshore toward the Arabian Sea.

Keywords: ROMS modeling, effluent desalination, salinity, regional flows, hypothetical lake.

1- Introduction

Ensuring access to freshwater has become a major priority for many nations. For countries endowed with vast marine resources, seawater desalination represents a valuable opportunity to secure reliable water supplies. However, global water security has deteriorated due to rising demand driven by population growth, along with pollution and climate change, which collectively diminish available freshwater reserves (Jones et

Cite this article: Hosseini Hamid,M. , Akbari Nasab,M. and Layeghi,B. (2025). Investigating the Influence of Salinity and Temperature on the Dispersion of Desalination Brine in a Hypothetical Lake. (e239403). *Nivar*, *49*(Special Issue (S1)), e239403 doi: 10.30467/nivar.2026.570770.1366

E-mail: (2) m.akbarinasab@umz.ac.ir (3) layeghi2001@yahoo.com

Publisher: Iran Meteorological Organization
DOI: https://doi.org/10.30467/nivar.2026.570770.1366

Print ISSN: 1735-0565
Online ISSN: 2645-3347

profiles were analyzed to assess dispersion patterns.

Purnallana et al. (2003) conducted a two-dimensional simulation of a desalination plant in Oman and reported that brine discharged into the sea propagates parallel to the shoreline, with salinity increasing toward the coast. Siyouf et al. (2014) used the three-dimensional non-hydrostatic ELCOM model to simulate ocean conditions in the Sea of Oman using winter field data (March 3–April 4, 2005). The broader Persian Gulf, Sea of Oman, and northern Arabian Sea were included to minimize boundary influence from Gulf outflow and Indian Ocean inflow. Their results showed strong agreement between modeled and observed temperature patterns (Siyouf et al., 2005). Zamani et al. (2013) investigated physical properties of the waters around Chabahar, Iran, using the COHERENS model and field measurements. Their results indicated that Sea of Oman waters are generally warmer than those in Chabahar Bay during cold seasons, with the opposite occurring in warm seasons; moreover, temperature consistently decreases from surface to seabed. Except during monsoon season, salinity in the bay is higher than offshore waters, primarily due to shallow depths and high evaporation. Given the hydrodynamic connection between the Persian Gulf and the Sea of Oman, brine can be transported between these basins, making circulation patterns a crucial consideration for desalination plant planning. Sadrinasab et al. (2010) showed that surface waters from the Sea of Oman enter the Persian Gulf through the Strait of Hormuz along Iran's coastline, while denser Gulf waters exit toward Oman at depth.

In a doctoral dissertation, Yan et al. compared several numerical models developed for the Persian Gulf and selected the most suitable one for simulating long-term salinity changes under climatic and anthropogenic influences. Treating the Gulf as a large estuarine system, they concluded that regional salinity will continue to rise in the long term—representing the first multi-

al., 2019). Consequently, most countries have increasingly focused on exploiting all conventional water resources—an issue that poses a significant challenge for the future of humanity and requires urgent solutions (Panagopoulos et al., 2019). Desalination technologies are currently regarded as among the most effective means of producing freshwater in many parts of the world (Blanco et al., 2017). Since freshwater accounts for only 3% of the planet's total water resources and conventional sources are depleting at an alarming rate, the expansion of energy-efficient desalination systems has become essential (Liu et al., 2023).

Multiple methods are used for seawater desalination (Khan et al., 2023), with thermal technologies (Mazhar et al., 2011; Cooley et al., 2006) and reverse osmosis (Miller et al., 2015; Al-Aimani, 2023) being the most widely applied. Global desalination capacity increased from 95.6 million m^3/day in 2016 to 99.8 million m^3/day in 2017 (Al-Kaabi & Mackey, 2019), with the highest concentrations of facilities located in Middle Eastern coastal nations (Jashia et al., 2007). Although desalination provides an unlimited and continuous source of freshwater, achieving sustainable production remains challenging (Al-Kaabi & Mackey, 2019). Environmental concerns—particularly the impacts of brine discharge on coastal waters—are also frequently overlooked (Jashia et al., 2007).

In the present study, a hypothetical lake was defined to examine the effects and dispersion behavior of brine under various discharge conditions. For reverse osmosis facilities, the salinity of discharged brine can typically reach up to twice the salinity of seawater (Kampf et al., 2009). For thermal desalination scenarios, outfall temperature must be considered higher than ambient sea-surface temperature. Understanding brine transport and dispersion is critical for protecting local ecosystems, as brine discharge can fundamentally alter marine habitats. To investigate these issues, the study domain was numerically modeled, a brine source was introduced, and both vertical and horizontal

2- Methodology

This study is based on numerical modeling of the marine environment using relevant hydrodynamic parameters, with the objective of investigating the dispersion of desalination brine under varying salinity (Badr et al., 2015) and temperature conditions. The spatial distribution of the discharged brine column—including its mixing environment, flow direction, and buoyancy—depends on discharge volume and velocity. The ecological impacts of saline effluent on coastal species are well documented and represent a major environmental concern (Petersen et al., 2018).

Accordingly, the research was conducted in two stages. First, an idealized rectangular domain was defined to assess the behavior of brine under different salinity and discharge scenarios. Next, a brine source was positioned along the Sea of Oman coastline to track plume movement during the winter season.

2.1. Idealized Domain

Figure 1 illustrates the three-dimensional ROMS (Regional Ocean Modeling System) setup used to simulate brine dispersion in an idealized rectangular basin representing an artificial lake with dimensions 200 km × 48.5 km. The computational grid consisted of 39 cells along the longitudinal axis and 68 cells along the transverse axis. Based on Courant number constraints and the spatial resolution of the domain, a time step of 120 seconds was selected for the simulations.

The bathymetry was defined with a constant, gentle slope and a maximum depth of 150 m. The mean density of the lake water was set to 1025 kg/m³, with a buoyancy frequency of 5×10^{-12} s^{-2}. The vertical turbulence parameterization included a vertical diffusivity coefficient of 5×10^{-6} m^2/s. Surface temperature and salinity were initialized at 28°C and 35 ppt, respectively.

The vertical structure was represented using 13 terrain-following layers. A surface brine outfall was introduced at grid location (i = 1, j = 50), with a discharge rate of 1–2 m^3/s, depending on the scenario. Multiple simulations were then conducted by varying brine discharge temperature, salinity, and flow rate to evaluate the resulting plume dynamics under different hypothetical desalination plant conditions.

decadal modeling study of its kind (Yan et al., 2015).

Al-Barouni et al. conducted a two-dimensional simulation of a desalination plume along the southern Oman Sea coastline under tidal forcing, and found that substantial accumulation of saline effluent occurs along the shore (Al-Barouni et al., 2009).

Balouchi (2013) simulated the brine discharge from the Bandar Abbas desalination plant using the three-dimensional COHERENS model, examining both salinity and thermal effects for RO and thermal systems in two locations. In the eastern region, brine was transported westward toward Qeshm Island, whereas in the western region it was advected toward the Qeshm Channel and Tangeh-Varan.

Marraccini et al. (2010) investigated the ecological impacts of brine discharge on a protected coastal habitat near Brindisi, Italy, using the three-dimensional MIKE hydrodynamic model. Their analysis revealed that elevated salinity in coastal waters threatens sensitive plant species. When brine twice as saline as seawater was discharged, simulated salinity fields showed plume propagation toward the southern coastline due to wind-driven currents—highlighting that plume behavior was more strongly influenced by wind direction than by outfall size.

Purnellana et al. (2012) used the CORMIX model to evaluate brine discharge from two power and desalination plants (Barka 1 and 2) constructed in 2003 and 2008 in Oman. Modeling and buoy data suggested that brine generally sinks toward the seabed; however, uncertainties in input parameters led to varying results in two discharge scenarios. Nonetheless, environmental standards were met within 150 m of the outfall.

In the present study, the ROMS model was adopted to simulate brine discharge under multiple scenarios in order to assess brine dispersion and the key factors influencing its behavior.

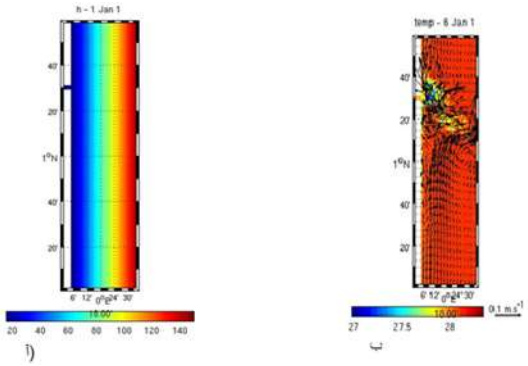

Figure 1. (a) Bathymetric map of the artificial lake, and (b) the eastward wind forcing applied over the domain.

2.2. Coast of the Sea of Oman

Following the assessment of brine dispersion in the idealized rectangular basin, the study proceeded to examine brine transport along the coastline of the Sea of Oman. Pollutants discharged into this region may be advected by local and regional currents toward other coastal zones, where they may accumulate; large-scale numerical modeling provides an effective tool for predicting such transport pathways (Suwari et al., 2006).

The Sea of Oman is significantly deeper than the Persian Gulf. Around Chabahar, depths reach approximately 3398 m, while toward the west the depth decreases rapidly, reaching 73 m near the Strait of Hormuz (Safargholi et al., 2015). Therefore, the potential advection of brine toward the Persian Gulf may pose environmental risks, highlighting the need for careful tracking and analysis of brine movement.

For this part of the study, the three-dimensional ROMS model was implemented using initial and boundary condition files generated by ROMS-Agrif within the MATLAB environment. Input datasets were obtained from authoritative sources, converted into NetCDF format, and supplied to ROMS as initial and boundary conditions. The hydrodynamic model was then executed over a structured grid suitable for both deep and shallow regions.

A high-resolution C-grid configuration with 13 vertical layers was applied, allowing detailed examination of plume behavior at various depths. The lowest layer corresponded to the maximum depth of the Sea of Oman (3394 m), and vertical resolution increased progressively toward the surface, enabling accurate representation of near-surface and subsurface plume dynamics (Figure 2).

Seafloor bathymetry was derived from the ETOPO1 dataset with a spatial resolution of 2 km, and initial condition data were obtained from the WOA (World Ocean Atlas) dataset (Table 1)

Table 1. Data sources used for preparing ROMS model inputs

Application	Data Source	Initial & Boundary Condition Files
Grid	–	*Roms_grid.nc*
Initial fields	WOA98 & Ingrid.ldgo.colombia.edu	*Roms_ini.nc*
Forcing	Atlas of Surface Marine Data (1994)	*Roms_forcing.nc*
Climatology / Atmospheric data	WOA98 & Ingrid.ldgo.colombia.edu	*Roms_clim.nc*
Boundary conditions	WOA98	*Roms_bry.nc*

The target domain was discretized using a 0.05° × 0.05° horizontal grid spacing (approximately 2 km × 2 km). The model was initialized with a mean seawater density of 1025 kg/m³, a vertical diffusivity coefficient of 5×10^{-6} m²/s for temperature and salinity, and a linear bottom drag coefficient of 3×10^{-4}.

With this configuration, the computational grid consisted of 249 points in the longitudinal direction and 248 points in the latitudinal direction. The hypothetical desalination plant outfall was positioned at grid location (i = 107, j = 139) (Figure 2).

The model was then executed with a 10-second time step, producing outputs for a one-year simulation corresponding to the year 2000. In this setup, brine discharged from a reverse osmosis facility was released at the sea surface with a temperature of 30°C, salinity of 70 psu, and a discharge rate of 10 m³/s (Hosseini et al., 2017).

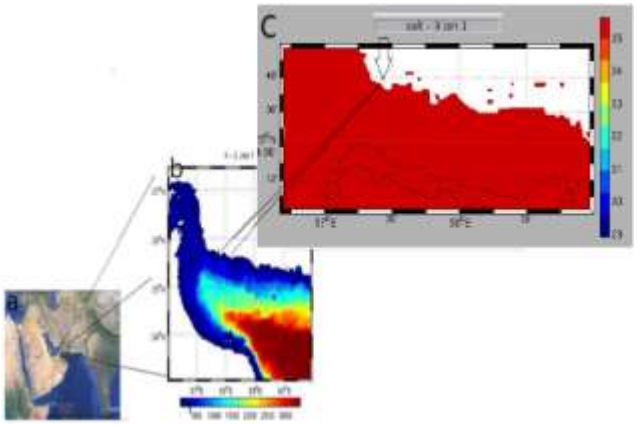

Figure 2.(a) Location of the surface brine discharge point within the model domain, (b) Bathymetry of the Sea of Oman, and (c) Selected outfall position along the coast at the sea surface.

Model output indicated that the simulated sea-surface temperature near Chabahar on 1 January (12 Dey) was 23.7°C. Based on in-situ measurements recorded by the National Institute of Oceanography of Iran on 7 Dey 1392, the observed temperature was 23°C, corresponding to a relative error of 3%. Similarly, the model produced a salinity value of 36.5 psu along the Chabahar coast on 22 January (3 Bahman). Field observations for 1 Bahman reported a salinity of 36.3 psu, yielding a relative error of 5%.

The ROMS ocean model offers high physical accuracy and flexibility, enabling applications in both deep and shallow marine environments. It incorporates multiple vertical mixing schemes, nested and composite grids, and multi-level vertical coordinates. ROMS is a fully three-dimensional numerical model developed for studying the atmosphere, ocean, climate, sea ice, sediment transport, waves, and coastal processes. Due to its nonhydrostatic formulation, ROMS can resolve a wide range of phenomena—from small-scale current intrusions to basin-scale and global circulation. The model employs an explicit discretization scheme and uses a high-resolution C-grid staggering approach.

ROMS solves the Navier–Stokes equations for an incompressible fluid on a rotating Earth, assuming constant friction coefficients. These governing equations, similar to those in other ocean circulation models, are expressed as follows:

$$\frac{\partial u}{\partial t}+\vec{v}.\nabla u-fv=-\frac{\partial \phi}{\partial x}-\frac{\partial}{\partial z}\left(\overline{u'w'}-v\frac{\partial u}{\partial z}\right)+F_u+D_u$$

$$\frac{\partial v}{\partial t}+\vec{v}.\nabla v+fu=-\frac{\partial \phi}{\partial y}-\frac{\partial}{\partial z}\left(\overline{v'w'}-v\frac{\partial v}{\partial z}\right)+F_v+D_v$$

$$\frac{\partial C}{\partial t}+\vec{v}.\nabla C=-\frac{\partial}{\partial z}\left(\overline{C'w'}-v_\theta\frac{\partial C}{\partial z}\right)+F_c+D_c$$

$$\frac{\partial \phi}{\partial z}=-\frac{\rho g}{\rho_\circ}$$

$$\frac{\partial u}{\partial x}+\frac{\partial v}{\partial y}+\frac{\partial w}{\partial z}=\circ$$

$$S(x,y,\sigma)=\frac{h_c\sigma+h(x,y)C(\sigma)}{h_c+h(x,y)}$$

$$z(x,y,\sigma,t)=S(x,y,\sigma)+\zeta(x,y,t)\left[1+\frac{S(x,y,\sigma)}{h(x,y)}\right]$$

The variables *D, F, f, g, h, kc, km, S, T, t, u, v,* and *w* represent, respectively, vertical velocity, eastward velocity, northward velocity, time, potential temperature, salinity, vertical diffusivity coefficient, salinity diffusivity coefficient, elevation, gravitational acceleration, Coriolis force, force, and diffusion.

The model output, obtained under conditions similar to those of the study conducted by Hetland and implemented over a rectangular domain, was consistent with the results shown in Figure (4).

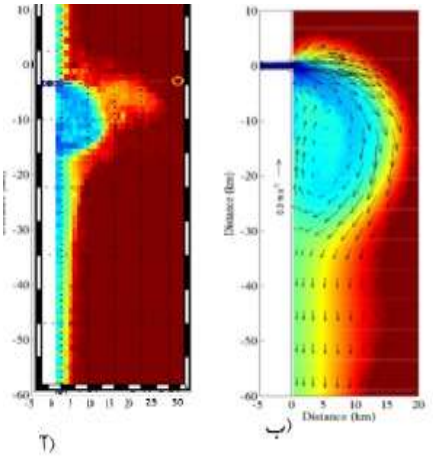

Figure 4. (a) Output of the present study and (b) output of the Hetland study; the dispersion patterns in both cases are identical.

3. Measurement, Observation, and Computation

3-1. Hypothetical Environment

3-1-1. First Scenario: Effluent with Salinity of 40 ppt

characteristics of the discharged effluent are presented in Figure 4. The effluent, with a temperature of 50 °C and a salinity of 40 ppt, was released on the fifth day at a discharge rate of 2 m^3/s. Figure 3-5 illustrates (a) a vertical cross-section of thermal dispersion, (b) a horizontal cross-section of surface thermal dispersion, and (c) a vertical cross-section of salinity dispersion in the study area. As observed, thermal dispersion propagates not only vertically but also along the coastline and in the direction of the prevailing wind.

Given the presence of an alternating north–south current in the region, its influence on the distribution of heat along the shoreline and toward the western boundary is clearly evident, causing the effluent plume to migrate toward adjacent coastal areas. In the vertical cross-section of salinity (c), the effluent does not settle on the bed of the basin and is distributed solely within the surface layer of the water body.

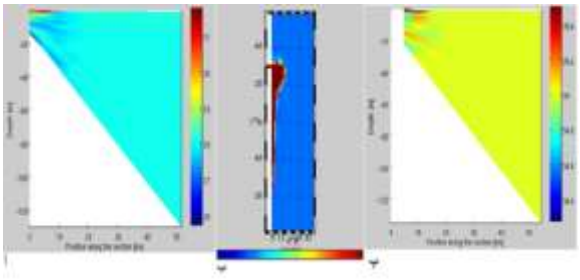

Figure 5. illustrates (a) a vertical cross-section of effluent temperature, (b) a horizontal cross-section of effluent thermal dispersion at the surface, and (c) a vertical cross-section of salinity transport on the fifth day.

3-1-2. Second Scenario: Effluent with Salinity of 45 ppt

In the second scenario, the effluent salinity was increased from 40 ppt to 45 ppt. Figure 5 presents the thermal output of the area on days 5, 10, 25, and 30. These figures show that the effluent initially advanced toward the eastern boundary up to a certain distance and then, due to the presence of the defined north–south wind-driven current in the region, it rotated and persisted along the coastal areas.

Although the initial progression of the effluent was similar to the previous scenario, by the end of the period its return flow was greater, resulting in higher accumulation in two coastal zones. These changes are illustrated in Figure 6b and 6c on days 25 and 30, respectively.

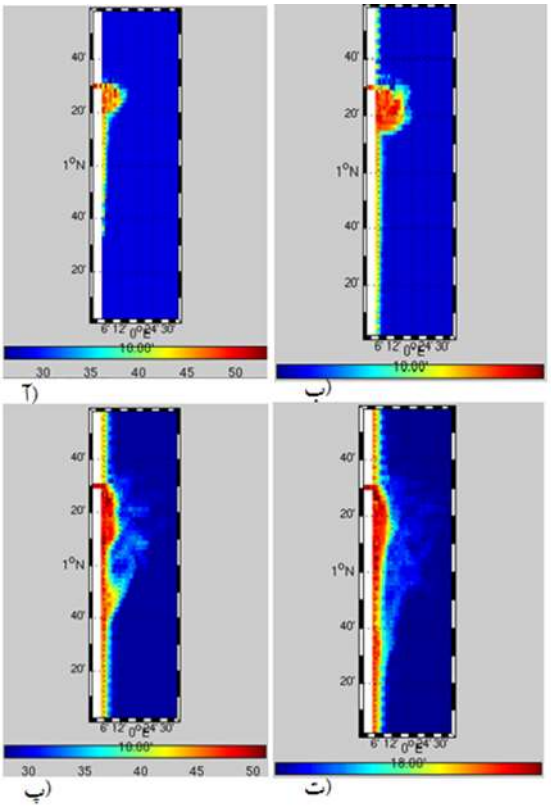

Figure 6.(a) shows the thermal distribution of the effluent on day 5, while Figures 6(b), 6(c), and 6(d) illustrate the temperature distribution on days 10, 25, and 30, respectively.

Figures 6(a) and 6(b) depict the heat penetration of the discharged water up to 50 meters from the source on days 5 and 10, whereas Figures 6(c) and 6(d) illustrate the penetration and spreading of the effluent under the influence of regional wind currents on days 25 and 30. Examination of these vertical sections at different times shows that, over time, due to increased density and interaction with the currents and high flow rate, salinity accumulates in two coastal areas parallel to the shoreline, with penetration into deeper water at these locations. These two accumulation zones were not present in the first scenario and are attributed to the increase in effluent salinity, compared to the previous case with a salinity of 40 ppt. This deep penetration becomes apparent in the figures from time step 30 onward

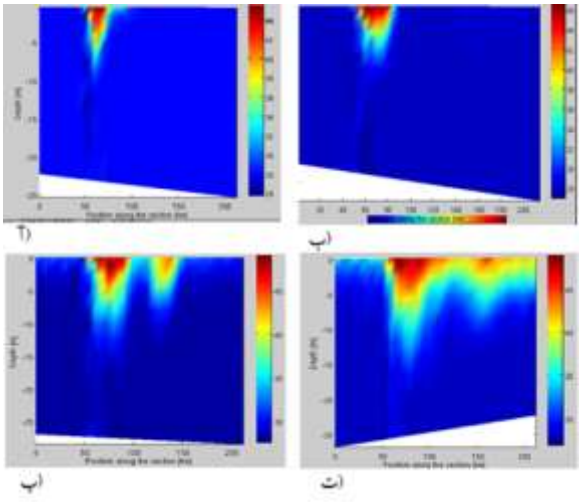

Figures 7(a) and 7(b) show the heat penetration of the discharged water up to 50 meters from the source on days 5 and 10, while Figures 7(c) and 7(d) illustrate the penetration and spreading of the effluent under the influence of regional currents on days 25 and 30.

In Figures 7(c) and 7(d), due to the progression and dispersion of the effluent, the salinity is lower compared to Figures 7(a) and 7(b). This phenomenon is further illustrated by vertical sections of the regional salinity, as shown in Figure 8

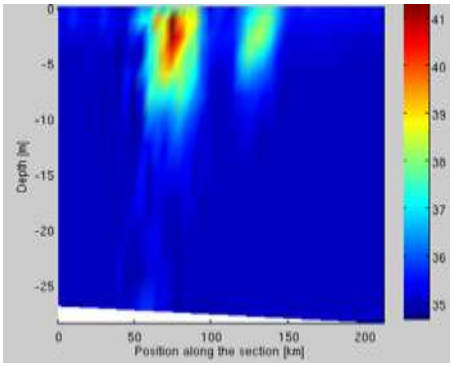

Figure 8. illustrates the decrease in salinity as the effluent advances in the lake

3.1.3 Scenario 3: Effluent with 55 ppt Salinity

In this scenario, the characteristics of the outfall were set at a temperature of 45 °C and a salinity of 55 ppt. This salinity level is a plausible value for the discharge of a desalination plant. The effluent flow rate was assumed to be 1 m^3/s. Figure 9 shows the penetration of the high-

salinity effluent toward the lake bed in terms of (a) temperature and (b) salinity on day 25. Compared to previous cases, the model output in this scenario exhibits significant changes, as the effluent, due to its increased density and weight, moved along the lake bed. Prolonged persistence of such high-density effluent can pose a serious threat to the benthic ecosystem of the lake

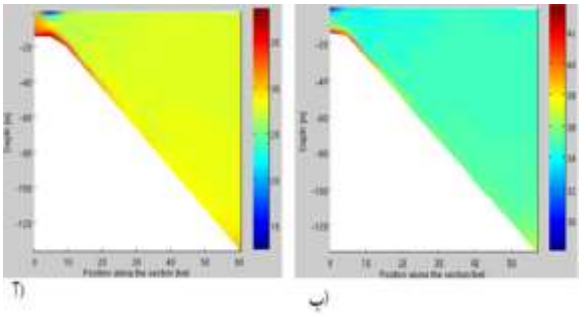

Figure 9. illustrates the penetration of high-salinity effluent along the lake bed in terms of (a) temperature and (b) salinity on day 25.

2.3 Oman Sea

From the models presented in Section 3.1, it can be concluded that the movement of effluent depends on factors such as the concentration of the discharged effluent, seabed topography, and other factors affecting ocean currents. Regional currents continuously transport water masses between the Indian Ocean, the Oman Sea, and the Persian Gulf. Accordingly, the prevailing current in the Oman Sea is northward (Lashki et al., 2019).

In addition, large-scale rotational currents exist in this region due to the presence of seasonal monsoons and upwelling phenomena. The dispersion of the discharged effluent is influenced not only by these oceanographic phenomena and seabed topography but also by the concentration of the effluent. Higher-density effluent tends to move more toward deeper layers and the seabed (Table 2).

Table 2. Effluent distribution relative to changes in density and temperature

Effluent Salinity (ppt)	Effluent Temperature (°C)	Effluent Distribution in the Sea
40	50	Distributed in various layers
45	45	Mostly near the seabed
55	45	Along the seabed

In Figure 10, the effluent was discharged at the sea surface along the western coast of Oman. On day 20, the effluent mass moves with the northward current toward the Strait of Hormuz. Over the long term, this movement could allow the effluent to pass through the Strait of Hormuz and reach the shallow coastal areas of the Persian Gulf.

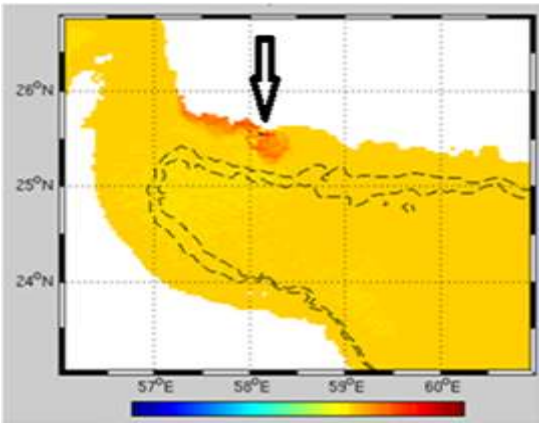

Figure 10. illustrates the distribution of the effluent on day 20 after discharge. The pattern of effluent dispersion is northward, moving toward the Strait of Hormuz.

In Figure 11, the effluent enters a large-scale regional cyclone and begins to circulate southward in the Oman Sea. This circulation effectively moves the pollution away from the Iranian coastline.

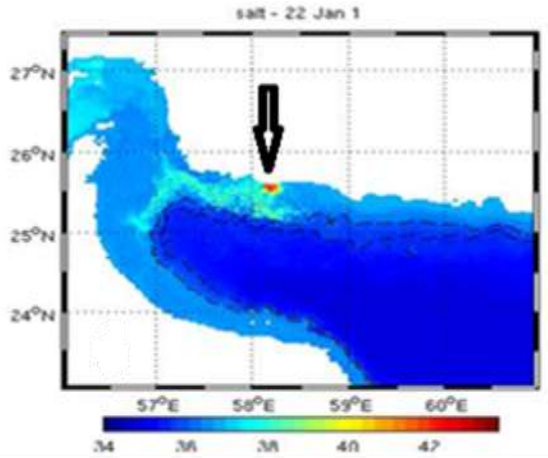

Figure 11. illustrates the effluent distribution pattern after 22 days. Part of the effluent moves toward the Strait of Hormuz, while another portion follows a rotational path toward the Arabian Sea.

Regional currents cause the surface effluent to split into two branches. The portion passing through the Strait of Hormuz can reach the coasts of the Persian Gulf, whereas the portion that begins to circulate can be transported away from the Iranian coast as it enters the Arabian Sea.

4.Discussion

By 2020, approximately 90% of global desalination capacity was achieved through thermal and membrane-based processes. In 2020, interest in reverse osmosis (RO) technology surpassed other methods, with more than 60% of seawater desalination being carried out using RO and nearly 27% using thermal methods such as multi-stage flash (MSF) (Jafarinjad, 2017).

The density of effluent from reverse osmosis is significantly higher than that from thermal methods. Therefore, if this type of effluent is discharged at depth, it tends to settle on the seabed. When discharged at the surface, part of the effluent is transported by local currents, while another portion moves toward the seabed and deposits.

Furthermore, if this type of effluent is discharged at the sea surface, part of it is transported by local currents, while another portion moves toward the seabed and settles. Along the northern Oman Sea, surface discharge can contaminate both the surface and the seabed. Effluent reaching the seabed, if located along a sloped path, can be transported away from the discharge area. For sedimentation to occur, the effluent salinity must exceed 55 ppt. In the conducted modeling, this high-density effluent moved toward the seabed. If the discharge location is selected in a region with an appropriate slope (Nerth, 2022), the effluent can be directed toward the deeper parts of the Oman Sea (Figure 12).

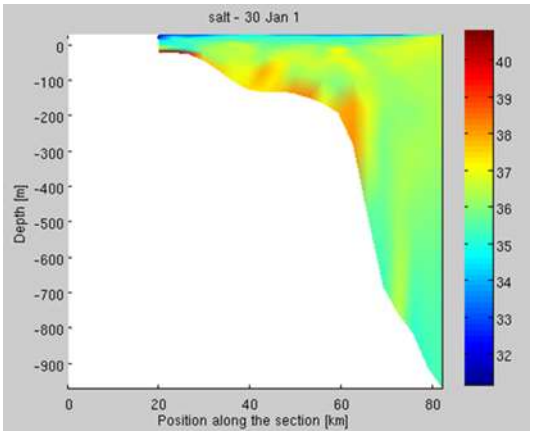

Figure 12. illustrates the penetration of reverse osmosis (RO) effluent discharged along the western coast of the Oman Sea, reaching a depth of 500 meters on day 30 after discharge

5. Conclusion

The discharge of effluent from seawater desalination plants can pose a serious threat to marine ecosystems (Campos et al., 2020). Salinity is one of the key limiting factors in the growth and efficiency of desalination plants (Badr et al., 2015). Salinity directly affects water quality, as increasing salinity reduces the quality of the produced drinking water. High salinity also increases water turbidity, which limits light penetration and interferes with the photosynthesis of marine plants. Furthermore, elevated salt concentrations along coastal areas reduce the number of local plankton, while crabs and other marine invertebrates, sensitive to salinity changes, may leave the area. Conversely, species more tolerant to high salinity, such as diatoms, may proliferate. In

addition, variations in salt concentration play an important role in the development and population dynamics of aquatic organisms (Miri and Shiukhi, 2005).
The density of the discharged effluent plays a critical role in its distribution both at the surface and in deeper layers of the sea. When effluent density exceeds 40 ppt, its penetration into deeper water increases, and at 55 ppt salinity, a significant portion of the effluent moves toward the seabed.

In thermal desalination technologies, where effluent salinity is lower than in reverse osmosis (RO) methods (Shokri and Imanifard, 2023), most of the effluent remains at the surface. Its dispersion is largely influenced by wind and other physical parameters of ocean currents. For example, if effluent is discharged along the western coast of the Oman Sea, it may follow two branches within the northward current, potentially contaminating parts of the Persian Gulf coast. In RO technology, due to the high salinity, a large portion of the effluent settles on the seabed. When high-density effluent is discharged into the sea, its weight causes it to sink into deeper layers and deposit on the seabed, potentially creating environmental problems for benthic marine plants. If the discharge location has a suitable slope, the dense effluent can be transported away from the coastal area. However, if the seabed slope is inadequate, the effluent accumulates locally on the seabed, which can alter the benthic ecosystem.
Accumulation of high-salinity effluent on the seabed can cause the death of local aquatic organisms, while other species may leave the area and new species may enter. In the Persian Gulf, increased salinity at the seabed can lead to the mortality of coral reefs.

References

1. Al-Barwani, T., Chapman, D. W., & Ameen, H., 2009. Strategic brain drain: Implications for higher education in Oman. Higher Education Policy, 22(4), 415-432.
2. Al-Kaabi, A. H., & Mackey, H. R., 2019. Environmental assessment of intake alternatives for seawater reverse osmosis in the Arabian Gulf. Journal of Environmental Management, 242, 22-30.
3. Bader, B., Aissaoui, F., Kmicha, I., Salem, A. B., Chehab, H., Gargouri, K., ... & Chaieb, M., 2015. Effects of salinity stress on water desalination, olive tree (Olea europaea L. cvs ‘Picholine’, ‘Meski’ and ‘Ascolana’) growth and ion accumulation. Desalination, 364, 46-52.
4. Baluchi, S., 2013. Modeling the dispersion of pollution from the Bandar Abbas desalination plant effluent. M.Sc. Thesis, Department of Marine Physics, University of Hormozgan, February.
5. Blanco-Marigorta, A. M., Lozano-Medina, A., & Marcos, J. D., 2017. A critical review of definitions for exergetic efficiency in reverse osmosis desalination plants. Energy, 137, 752-760.
6. Campos, E. J., Vieira, F., Cavalcante, G., Kjerfve, B., Abouleish, M., Shahriar, S., ... & Gordon, A. L., 2020. Impacts of brine disposal from water desalination plants on the physical environment in the Persian/Arabian Gulf. Environmental Research Communications, 2(12), 125003.

7. Cooley, H., Gleick, P. H., & Wolff, G., 2006. Desalination, with a grain of salt. A California Perspective: Pacific Institute for Studies in Development, Environment and Security: Oakland, California.
8. El Aimani, S., 2023. Modeling of Reverse Osmosis Water Desalination Powered by Photovoltaic Solar Energy. Green Energy and Environmental Technology.
9. Gacia, E., Invers, O., Manzanera, M., Ballesteros, E., & Romero, J., 2007. Impact of the brine from a desalination plant on a shallow seagrass (Posidonia oceanica) meadow. Estuarine, Coastal and Shelf Science, 72(4), 579-590.
10. Hosseini Hamid, M., Akbari Nasab, M., & Laeghi, B., 2017. Numerical modeling of industrial desalination effluent dispersion in the northern Oman Sea. M.Sc. Thesis, University of Mazandaran.
11. Jafarinejad, S., 2017. A comprehensive study on the application of reverse osmosis (RO) technology for the petroleum industry wastewater treatment. Journal of Water and Environmental Nanotechnology, 2(4), 243-264.
12. Jones, E., Qadir, M., van Vliet, M. T., Smakhtin, V., & Kang, S. M., 2019. The state of desalination and brine production: A global outlook. Science of the Total Environment, 657, 1343-1356.
13. Kämpf, J., Brokensha, C., & Bolton, T., 2009. Hindcasts of the fate of desalination brine in large inverse estuaries: Spencer Gulf and Gulf St. Vincent, South Australia. Desalination and Water Treatment, 2(1-3), 335-344.
14. Khan, M. A., Shamsuzzaman, M., Labib, F., Islam, S., Mashira, M., & Al-Saad, M. A., 2023. Bangladesh's Sustainable Water Production Solutions: An Analysis of Different Methods. Authorea Preprints.
15. Lashkari, S., Soyuf Jahromi, M., & Hamzei, S., 2023. Seasonal changes of the Persian Gulf water mass in the Gulf of Oman. Journal of Oceanography, 14(53), 103-122.
16. Liu, W., Wei, L., Wu, L., & Zhang, Z., 2023. Research Progress on Desalination Technology Based on Ocean Energy. Frontiers in Power and Energy Systems, 2(1), 8-14.
17. Malcangio, D., & Petrillo, A. F., 2010. Modeling of brine outfall at the planning stage of desalination plants. Desalination, 254(1-3), 114-125.
18. Mezher, T., Fath, H., Abbas, Z., & Khaled, A., 2011. Techno-economic assessment and environmental impacts of desalination technologies. Desalination, 266(1-3), 263-273.
19. Miller, S., Shemer, H., & Semiat, R., 2015. Energy and environmental issues in desalination. Desalination, 366, 2-8.
20. Miri, R., & Chouikhi, A., 2005. Ecotoxicological marine impacts from seawater desalination plants. Desalination, 182(1-3), 403-410.
21. North, E., 2022. Physical modelling of desalination discharges impacting an inclined boundary.
22. Panagopoulos, A., Haralambous, K. J., & Loizidou, M., 2019. Desalination brine disposal methods and treatment technologies—A review. Science of the Total Environment, 693, 133545.
23. Petersen, K. L., Frank, H., Paytan, A., & Bar-Zeev, E., 2018. Impacts of seawater desalination on coastal environments. In Sustainable desalination handbook (pp. 437-463).

24. Purnalna, A., Al-Barwani, H. H., & Al-Lawatia, M., 2003. Modeling dispersion of brine waste discharges from a coastal desalination plant. Desalination, 155(1), 41-47.
25. Purnama, A., Al-Barwani, H. H., Bleninger, T., & Doneker, R. L., 2011. CORMIX simulations of brine discharges from Barka plants, Oman. Desalination and Water Treatment, 32(1-3), 329-338.
26. Sadri Nasab, M., 2010. Three Dimensional Numerical Modeling of Circulation in the Strait of Hormuz. Journal of Oceanography, 1(1), 19-24.
27. Shokri, A., & Fard, M. S., 2023. Techno-economic assessment of water desalination: Future outlooks and challenges. Process Safety and Environmental Protection, 169, 564-578.
28. Souari, L., & Hassairi, M., 2007. Sea water desalination by reverse osmosis: the true needs for energy. Desalination, 206(1-3), 465-473.
29. Yan, X., 2015. Numerical Simulation of the Long-term Balance of Salinity in the Persian Gulf. Doctoral dissertation, Université d'Ottawa/University of Ottawa.
30. Zamani, A., Samiee, J., & Kirby, J. F., 2013. Estimating the mechanical anisotropy of the Iranian lithosphere using the wavelet coherence method. Tectonophysics, 601, 139-147